

Three-Body Forces Produced by a Similarity Renormalization Group Transformation in a Simple Model

S.K. Bogner*

*National Superconducting Cyclotron Laboratory and Department of Physics and Astronomy,
Michigan State University, East Lansing, MI 48824*

R.J. Furnstahl[†] and R.J. Perry[‡]

Department of Physics, The Ohio State University, Columbus, OH 43210

(Dated: August, 2007)

Abstract

A simple class of unitary renormalization group transformations that force hamiltonians towards a band-diagonal form produce few-body interactions in which low- and high-energy states are decoupled, which can greatly simplify many-body calculations. One such transformation has been applied to phenomenological and effective field theory nucleon-nucleon interactions with success, but further progress requires consistent treatment of at least the three-nucleon interaction. In this paper we demonstrate in an extremely simple model how these renormalization group transformations consistently evolve two- and three-body interactions towards band-diagonal form, and introduce a diagrammatic approach that generalizes to the realistic nuclear problem.

PACS numbers: 21.30.-x, 05.10.Cc, 13.75.Cs

*Electronic address: bogner@nscl.msu.edu

[†]Electronic address: furnstahl.1@osu.edu

[‡]Electronic address: perry.6@osu.edu

I. INTRODUCTION

Wilsonian renormalization group transformations are designed to replace explicit coupling between disparate distance or energy scales with effective interactions in which disparate scales are decoupled [1]. In recent work we have employed a simple unitary renormalization group transformation to study the nucleon-nucleon (NN) interaction [2, 3, 4]. This transformation is a simplified version of Wegner's flow equations [5] and one of a much larger class of Similarity Renormalization Group (SRG) transformations developed by Glazek and Wilson [6]. The transformation leads to NN potentials for which calculations of few-nucleon binding energies and other observables converge rapidly [2, 3, 7]. However, further progress will require the consistent treatment of at least the three-nucleon interaction.

The basics of the unitary evolution are simply stated. Consider a unitary transformation U_s of a hamiltonian H ,

$$H_s = U_s H U_s^\dagger, \quad (1)$$

where s is a continuous flow parameter. We take $s = 0$ for the initial value with U_0 the identity transformation, so H is our input hamiltonian. We want to choose U_s so that H_s is diagonalized (band-diagonalized in more realistic cases) within a specified basis as $s \rightarrow \infty$, which will realize the desired decoupling of low- and high-energy states. Direct differentiation shows that H_s evolves according to

$$\frac{dH_s}{ds} = [\eta(s), H_s], \quad (2)$$

with

$$\eta(s) = \frac{dU_s}{ds} U_s^\dagger = -\eta^\dagger(s). \quad (3)$$

Choosing $\eta(s)$ specifies the unitary transformation. A simple choice is

$$\eta(s) = [T, H_s], \quad (4)$$

where T is a fixed matrix (independent of s), which gives the flow equation,

$$\frac{dH_s}{ds} = [[T, H_s], H_s]. \quad (5)$$

In Refs. [2, 3, 8] T was chosen to be the kinetic energy; here we choose the hamiltonian for free particles in an infinite square well. For explicit calculations we employ a basis in which T is diagonal and it is in this representation that H_s is driven towards band-diagonal form, as we will see below.

A principal advantage of SRG transformations is that all operators are consistently transformed, which means that all observables are invariant. For the simple unitary transformation this is obvious, simply because it is unitary. An additional advantage is that SRG transformations readily handle Fock space operators; indeed, Glazek and Wilson designed them to attack light-front quantum chromodynamics. Interactions that change particle number are not required for low-energy nuclear physics, but we do require the consistent evolution of all many-body operators. If we express the hamiltonian in terms of creation and destruction operators, it is evident that the commutators in Eq. (5) will generate many-body interactions even if H includes only a two-body interaction. In principle this could make practical calculations intractable, but in applications of interest (e.g., to nuclear physics)

we can choose transformations that maintain a hierarchy of many-body forces such that for sufficiently dilute many-body systems we only need to evolve few-body operators.

In this paper we illustrate how a unitary SRG consistently evolves two-body *and* three-body interactions. We choose what may be the simplest possible example of such evolution, bosons in a two-level system in which only two states are coupled in each of the two-particle and three-particle sectors. As a specific realization, we use a one-dimensional infinite square well with the Fock space truncated to allow only the two lowest modes. Despite the simplicity of the model, it exhibits many of the basic issues to be confronted in evolving few-body interactions and illustrates a diagrammatic formulation of the SRG equations that carries over to more realistic problems (such as nuclei).

In the severely truncated model space, the largest sub-matrix we will encounter is 2×2 ; so we start in Sect. II by reviewing the unitary transformation for the simple case of 2×2 matrices. In Sect. III we explicitly show in our simple example that the unitary evolution of hamiltonians containing two-body interactions must produce three-body interactions. We derive the explicit 2×2 matrices that represent the flowing two-body interaction, V_{2s} , and the positive parity part of the flowing three-body interaction, V_{3s} . In Sect. IV we develop simple diagrammatic rules for the production of evolution equations governing any N -body interaction, V_N , and show that these readily reproduce the equations for V_2 and V_3 in our simple model. The diagrammatic representation suggests several approximations that are tested. We summarize and make connections to nuclear physics and other problems of interest in Sect. V.

II. 2×2 MATRIX EVOLUTION

Let us start by considering a two-state system, with the hamiltonian represented by a 2×2 hermitian matrix. In realistic many-body quantum mechanics problems, we frequently encounter a hamiltonian that naturally divides, $H = T + V$, with T a one-body operator.¹ In this case, the unitary transformation

$$H_s = U_s T U_s^\dagger \equiv T + V_s \quad (6)$$

defines the evolved interaction V_s . In terms of basis states $|i\rangle$, where $T|i\rangle = E_i|i\rangle$, the flow equation is

$$\frac{d}{ds} V_{ij} = -(E_i - E_j)^2 V_{ij} + \sum_k (E_i + E_j - 2E_k) V_{ik} V_{kj} . \quad (7)$$

Here the renormalization flow parameter, s , has the dimension of inverse energy squared. The first term on the right-hand-side drives V , and therefore H , towards band-diagonal form as s increases from zero.

In our two-state example we will also take $H = T + V$ and use eigenstates of T as a basis, with $T|1\rangle = E_1|1\rangle$ and $T|2\rangle = E_2|2\rangle$. In this representation,

$$T = \begin{pmatrix} E_1 & 0 \\ 0 & E_2 \end{pmatrix} , \quad (8)$$

¹ There is considerable freedom in the choice of T , it need not even be a one-body operator. V can be initially chosen to be a two-body operator, but the commutators will then automatically generate three-body operators, four-body operators, etc.

and the full hamiltonian is

$$H_s = \begin{pmatrix} E_1 + V_{11}(s) & V_{12}(s) \\ V_{21}(s) & E_2 + V_{22}(s) \end{pmatrix}, \quad (9)$$

where $V_{ij}(s) \equiv \langle i|V_s|j \rangle$, which we take to be real. Any real symmetric 2×2 matrix can be expressed using the identity matrix, I , and the Pauli spin matrices, σ_x and σ_z ,

$$T = \mathcal{E}I + \Omega\sigma_z, \quad (10)$$

$$V_s = cI + \omega_z(s)\sigma_z + \omega_x(s)\sigma_x, \quad (11)$$

where $\mathcal{E} = \frac{1}{2}(E_1 + E_2)$, $\Omega = \frac{1}{2}(E_1 - E_2)$, $c = \frac{1}{2}(V_{11} + V_{22})$, $\omega_z(s) = \frac{1}{2}(V_{11} - V_{22})$ and $\omega_x(s) = V_{12} = V_{21}$. Since I commutes with all other matrices, \mathcal{E} and c drop out of the flow equations and c is therefore independent of s . So, we need only consider the Pauli spin matrices σ_z and σ_x to understand the real 2×2 hamiltonian. If an additional angle is introduced using σ_y , it turns out to be another flow constant that produces no qualitative change in the way the hamiltonian flows.

Dropping the constants \mathcal{E} and c , which can simply be added back in after the flow equations are solved, we work with

$$V_s = \omega_z(s)\sigma_z + \omega_x(s)\sigma_x, \quad (12)$$

and

$$T = \Omega\sigma_z. \quad (13)$$

With the above matrices, the unitary renormalization group flow equation (5) becomes

$$\frac{d}{ds} [\omega_z(s)\sigma_z + \omega_x(s)\sigma_x] = 4\Omega [\omega_x^2(s)\sigma_z - (\Omega + \omega_z(s))\omega_x(s)\sigma_x], \quad (14)$$

or, projecting out coefficients of the Pauli matrices,

$$\frac{d}{ds}\omega_z(s) = 4\Omega\omega_x^2(s), \quad \frac{d}{ds}\omega_x(s) = -4\Omega(\Omega + \omega_z(s))\omega_x(s). \quad (15)$$

These equations illustrate a tremendous advantage of such unitary transformations in that the exact renormalization group equations are only second order in V . Note that if $|\Omega| \gg |\omega_z(s)|$, $\omega_x(s)$ is obviously driven to zero exponentially.

The equations are easily solved analytically. We introduce the angle θ and set $\Omega + \omega_z = \omega \cos \theta$ and $\omega_x = \omega \sin \theta$, where $\omega = \sqrt{(\Omega + \omega_z)^2 + \omega_x^2}$. With this change of variables we find that ω is a flow constant, so only the angle θ depends on s . The flow equation becomes:

$$\frac{d\theta}{ds} = -4\Omega\omega \sin \theta. \quad (16)$$

Integrating this equation we obtain:

$$\tan\left(\frac{\theta(s)}{2}\right) = \tan\left(\frac{\theta(0)}{2}\right) e^{-4\Omega\omega s}. \quad (17)$$

Thus θ is driven exponentially either to zero or to π , depending on the sign of Ω . In either case the matrix is driven to diagonal form, with the states in the same order as in $\Omega\sigma_z$.

III. BOSONS IN A SQUARE WELL TRUNCATED TO TWO MODES

In this section we consider a simple concrete example that lets us examine SRG evolution in two-boson and three-boson sectors of Fock space. We choose T to be the hamiltonian for non-interacting bosons in an infinite square well where $-L/2 \leq x \leq L/2$,

$$T = \frac{P^2}{2m} + V_{\text{well}} . \quad (18)$$

We work in the T eigenstate basis,

$$\phi_n(x) = \sqrt{\frac{2}{L}} \sin \left(\frac{n\pi(x - L/2)}{L} \right) , \quad (19)$$

and truncate the boson Fock space to allow only the ground and first excited state modes. We will see that this drastic truncation reduces the two- and three-boson problems to 2×2 matrix problems, as solved in Sect. II.

After truncating to two modes, the complete set of eigenvalues of T are

$$E_1 = \frac{\pi^2}{2mL^2} , \quad E_2 = 4E_1 . \quad (20)$$

We can build many-body interactions using Fock-space operators and below we develop a Fock space diagrammatic analysis exploiting the simple algebra of these operators, but for pedagogical reasons we first compute matrix elements of the hamiltonian with two-body and three-body interactions mechanically. The interactions are given by their matrix elements between unsymmetrized two- and three-boson states, which must be related to matrix elements between properly symmetrized states. We choose an interaction that preserves parity and need only consider the three-dimensional two-boson space and the two-dimensional positive parity three-boson space to display the method.

It is convenient to use several bases for the many-boson problem, which we distinguish by the type of bracket used. Unsymmetrized three-boson states, for example, are $|n_1 n_2 n_3\rangle$, in which n_i 's denote the individual particle square-well states. We also use symmetrized states $|N_1 N_2\rangle$, in which N_1 is the number of bosons in the $n = 1$ state and N_2 the number in the $n = 2$ state. The only two-boson symmetrized states are $|20\rangle \equiv |a\rangle$, $|02\rangle \equiv |b\rangle$, and $|11\rangle \equiv |c\rangle$ and we only need the positive parity symmetric three-boson states, $|30\rangle \equiv |\alpha\rangle$ and $|12\rangle \equiv |\beta\rangle$.

We display the two-boson and three-boson states we need in Tables I–IV, listing their free energy and parity. We also list the symmetric states' representations in terms of unsymmetrized states, which we need to compute the initial hamiltonian. If the initial two-body interaction conserves parity, parity will be conserved in the evolution, so even and odd parity states will not mix. In general, any operator that commutes with T and H will commute with H_s and result in an explicit symmetry. Parity conservation simplifies both the two- and three-boson problems, reducing them to 2×2 matrix problems.

We will see that we must allow for an explicit three-body interaction, V_3 , without which the transformation cannot be unitary. If we set $V_3 = 0$ at $s = 0$, we will see that the unitary transformation generates a three-body interaction that maintains unitarity in the three-boson sector of Fock space. That is, we need $V_s = V_{2s} + V_{3s}$ here. In realistic cases we need to choose the transformation so that the induced part of these many-body interactions

TABLE I: **Two-boson unsymmetrized states**

$ n_1 n_2\rangle$	E_{n_1, n_2}	parity
$ 11\rangle$	$2E_1$	+
$ 22\rangle$	$8E_1$	+
$ 12\rangle$	$5E_1$	−
$ 21\rangle$	$5E_1$	−

TABLE II: **Two-boson symmetrized states**

$ N_1 N_2\rangle$	label	$ n_1 n_2\rangle$ -basis	E_{N_1, N_2}	parity
$ 20\rangle$	$ a\rangle$	$ 11\rangle$	$2E_1$	+
$ 02\rangle$	$ b\rangle$	$ 22\rangle$	$8E_1$	+
$ 11\rangle$	$ c\rangle$	$\frac{1}{\sqrt{2}}[12\rangle + 21\rangle]$	$5E_1$	−

TABLE III: **Positive parity three-boson unsymmetrized states**

$ n_1 n_2 n_3\rangle$	E_{n_1, n_2, n_3}	parity
$ 111\rangle$	$3E_1$	+
$ 122\rangle$	$9E_1$	+
$ 212\rangle$	$9E_1$	+
$ 221\rangle$	$9E_1$	+

TABLE IV: **Three-boson symmetrized states**

$ N_1 N_2\rangle$	label	$ n_1 n_2 n_3\rangle$ -basis	E_{N_1, N_2}	parity
$ 30\rangle$	$ \alpha\rangle$	$ 111\rangle$	$3E_1$	+
$ 12\rangle$	$ \beta\rangle$	$\frac{1}{\sqrt{3}}[122\rangle + 212\rangle + 221\rangle]$	$9E_1$	+
$ 21\rangle$	$ \gamma\rangle$	$\frac{1}{\sqrt{3}}[112\rangle + 121\rangle + 211\rangle]$	$6E_1$	−
$ 03\rangle$	$ \delta\rangle$	$ 222\rangle$	$12E_1$	−

TABLE V: **Initial matrix elements of V_2**

$\langle a V_2 a\rangle = \langle b V_2 b\rangle = 3g$
$\langle a V_2 b\rangle = 2g$
$\langle c V_2 c\rangle = 4g$
$\langle \alpha V_2 \alpha\rangle = 9g$
$\langle \beta V_2 \beta\rangle = 11g$
$\langle \alpha V_2 \beta\rangle = 2\sqrt{3}g$

remains short-ranged, which for fermions should allow us to truncate the tower of many-body operators and accurately solve many-fermion problems with evolved few-body operators only. The calculation here is easily extended to the four-boson sector of Fock space, where V_{4s} first appears, and so on. Restricting our attention to the two-boson and three-boson sectors, we must solve

$$\frac{dH_s}{ds} = [[T, V_{2s} + V_{3s}], T + V_{2s} + V_{3s}] . \quad (21)$$

Solving this in the two-boson sector completely determines V_{2s} and the three-boson sector then determines V_{3s} . Since particle number is conserved, we simply need to take two-boson or three-boson matrix elements of the flow equation and insert a complete set of states on the right-hand-side to obtain coupled nonlinear equations for each independent matrix element.

Two-boson matrix elements of the flow equation determine V_{2s} ,

$$\frac{d}{ds} \langle a|V_{2s}|a \rangle = -12E_1 \langle a|V_{2s}|b \rangle \langle b|V_{2s}|a \rangle , \quad (22)$$

$$\frac{d}{ds} \langle b|V_{2s}|b \rangle = 12E_1 \langle b|V_{2s}|a \rangle \langle a|V_{2s}|b \rangle , \quad (23)$$

$$\frac{d}{ds} \langle a|V_{2s}|b \rangle = -36E_1^2 \langle a|V_{2s}|b \rangle + 6E_1 [\langle a|V_{2s}|a \rangle - \langle b|V_{2s}|b \rangle] \langle a|V_{2s}|b \rangle . \quad (24)$$

There is no coupling between the positive and negative parity states for the interaction we will study and $\langle c|V_{2s}|c \rangle$ does not evolve because there is only one odd-parity two-boson state. We have seen in Sect. II that these equations have an analytic solution; to apply it we need only remove the part of H that is proportional to an identity matrix and determine Ω , $\omega_z(0)$ and $\omega_x(0)$ from what remains.

The three-boson evolution equations are readily computed using eq. (21),

$$\frac{d}{ds} \langle \alpha|V_{2s} + V_{3s}|\alpha \rangle = -12E_1 \langle \alpha|V_{2s} + V_{3s}|\beta \rangle \langle \beta|V_{2s} + V_{3s}|\alpha \rangle , \quad (25)$$

$$\frac{d}{ds} \langle \beta|V_{2s} + V_{3s}|\beta \rangle = 12E_1 \langle \beta|V_{2s} + V_{3s}|\alpha \rangle \langle \alpha|V_{2s} + V_{3s}|\beta \rangle , \quad (26)$$

$$\begin{aligned} \frac{d}{ds} \langle \alpha|V_{2s} + V_{3s}|\beta \rangle &= -36E_1^2 \langle \alpha|V_{2s} + V_{3s}|\beta \rangle \\ &\quad + 6E_1 \langle \alpha|V_{2s} + V_{3s}|\alpha \rangle \langle \alpha|V_{2s} + V_{3s}|\beta \rangle \\ &\quad - 6E_1 \langle \alpha|V_{2s} + V_{3s}|\beta \rangle \langle \beta|V_{2s} + V_{3s}|\beta \rangle . \end{aligned} \quad (27)$$

Here again we have a 2×2 matrix problem, so it also can be solved as shown in Sec. II. One way to find V_3 is to solve for $V_2 + V_3$ and then subtract matrix elements of V_2 that result from solving for V_2 in the two-boson sector. Instead, we will discuss a seemingly more complicated procedure that is required in more realistic examples where matrix elements of dV_2/ds in the three-boson sector produce momentum delta-functions due to non-interacting spectators.

We need symmetrized three-boson matrix elements of V_{2s} in terms of its symmetrized two-boson matrix elements, in order to embed the solution of eqs. (22)–(24) in eqs. (25)–(27). These are computed using unsymmetrized states given in Table III:

$$\langle \beta|V_{2s}|\beta \rangle = \langle b|V_{2s}|b \rangle + 2 \langle c|V_{2s}|c \rangle , \quad (28)$$

$$\langle \beta|V_{2s}|\alpha \rangle = \sqrt{3} \langle b|V_{2s}|a \rangle , \quad (29)$$

$$\langle \alpha|V_{2s}|\alpha \rangle = 3 \langle a|V_{2s}|a \rangle . \quad (30)$$

We can now rewrite all of the three-boson matrix elements of V_{2s} in terms of its two-boson matrix elements, then use the solution to eqs. (22)–(24) to rewrite the three-boson equations for V_{3s} :

$$\begin{aligned} \frac{d}{ds} \langle \alpha | V_{3s} | \alpha \rangle = & -12E_1 [\sqrt{3} \langle a | V_{2s} | b \rangle \langle \beta | V_{3s} | \alpha \rangle + \sqrt{3} \langle \alpha | V_{3s} | \beta \rangle \langle b | V_{2s} | a \rangle \\ & + \langle \alpha | V_{3s} | \beta \rangle \langle \beta | V_{3s} | \alpha \rangle] , \end{aligned} \quad (31)$$

$$\begin{aligned} \frac{d}{ds} \langle \beta | V_{3s} | \beta \rangle = & 12E_1 [2 \langle b | V_{2s} | a \rangle \langle a | V_{2s} | b \rangle \\ & + \sqrt{3} \langle b | V_{2s} | a \rangle \langle \alpha | V_{3s} | \beta \rangle + \sqrt{3} \langle \beta | V_{3s} | \alpha \rangle \langle a | V_{2s} | b \rangle \\ & + \langle \beta | V_{3s} | \alpha \rangle \langle \alpha | V_{3s} | \beta \rangle] , \end{aligned} \quad (32)$$

$$\begin{aligned} \frac{d}{ds} \langle \alpha | V_{3s} | \beta \rangle = & -36E_1^2 \langle \alpha | V_{3s} | \beta \rangle + 12E_1 \sqrt{3} (\langle a | V_{2s} | a \rangle - \langle c | V_{2s} | c \rangle) \langle a | V_{2s} | b \rangle \\ & + 6E_1 [(\langle \alpha | V_{3s} | \alpha \rangle - \langle \beta | V_{3s} | \beta \rangle) \sqrt{3} \langle a | V_{2s} | b \rangle + \\ & (3 \langle a | V_{2s} | a \rangle - \langle b | V_{2s} | b \rangle - 2 \langle c | V_{2s} | c \rangle) \langle \alpha | V_{3s} | \beta \rangle] \\ & - 6E_1 (\langle \alpha | V_{3s} | \alpha \rangle - \langle \beta | V_{3s} | \beta \rangle) \langle \alpha | V_{3s} | \beta \rangle . \end{aligned} \quad (33)$$

There is no obvious simplification here, quite the contrary. Replacing matrix elements of V_2 with their solutions from the two-boson sector complicates the equation, but we will return to this issue after developing a diagrammatic analysis. It is no longer obvious that this is another 2×2 matrix example and it is far more tedious to find an analytic solution, but once again the entire hamiltonian is driven to diagonal form, which requires V_2 and V_3 to be separately driven to diagonal form.

For an explicit demonstration problem that can be exactly solved and readily extended, we choose a zero-range initial interaction:

$$V_2(x_i, x_j) = 2Lg \delta(x_i - x_j) . \quad (34)$$

Note that for $g > 0$ this is repulsive. Matrix elements of V_2 between unsymmetrized states are:

$$\begin{aligned} (n_1 n_2 | V_2 | n_3 n_4) = & g [\delta_{0, n_1 - n_2 + n_3 - n_4} + \delta_{0, n_1 - n_2 - n_3 + n_4} \\ & - \delta_{0, n_1 - n_2 + n_3 + n_4} - \delta_{0, n_1 - n_2 - n_3 - n_4} - \delta_{0, n_1 + n_2 + n_3 - n_4} \\ & - \delta_{0, n_1 + n_2 - n_3 + n_4} + \delta_{0, n_1 + n_2 - n_3 - n_4}] . \end{aligned} \quad (35)$$

From these we readily compute the initial interaction matrix elements for symmetrized states, which are given in Table V.

In figs. 1 and 2 we plot two-boson matrix elements of V_{2s} and three-boson matrix elements of V_{3s} , for weak and strong couplings. We contrast flow for $g = -0.1$ and $g = -3.0$, showing unitary renormalization group evolution as a function of s . The energy scale is set by choosing $E_1 = 1$.

The trace of V_2 in the two-boson sector is fixed, so we always see one diagonal matrix element increase and the other decrease. Since the off-diagonal matrix element must die

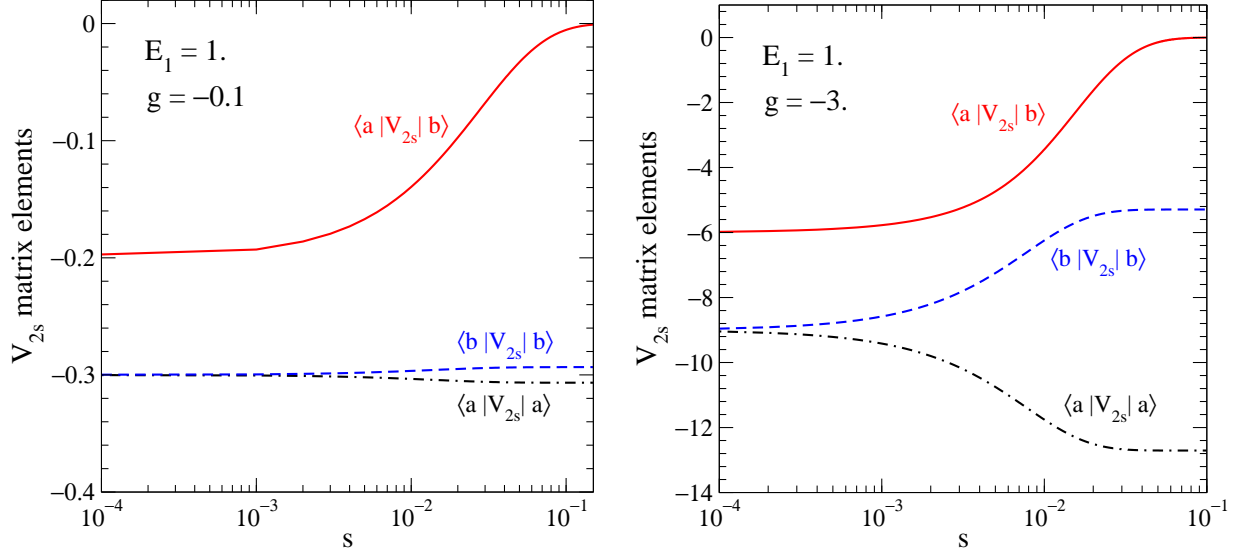


FIG. 1: Hamiltonian matrix elements of V_2 as a function of the flow parameter s in the two-boson sector for weak and strong couplings.

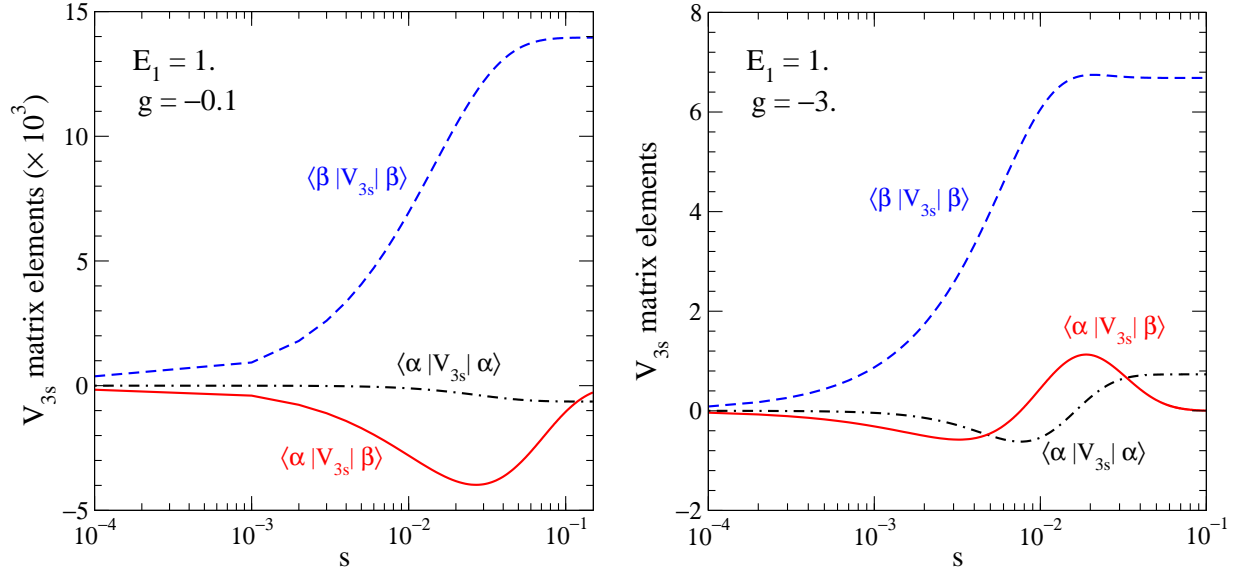


FIG. 2: Hamiltonian matrix elements of V_3 as a function of the flow parameter s in the three-boson sector for weak and strong couplings.

exponentially, it is not surprising to find similarity in fig. 1 of how V_2 flows for strong and weak coupling. For $g = -0.1$ the rate of exponential convergence is controlled by the linear term on the right-hand-side of eq. 24, while for $g = -3.0$ the second-order term contributes significantly. This will be detailed in the next section. To compare this flow with that of a 2×2 matrix, note that here $\Omega = -3E_1$ and for weak coupling the exponent will be approximately $36s$, which is why we see convergence by the time $s \approx 0.1$. Convergence improves as the coupling increases, but the range of s over which convergence is seen will not change drastically until g is orders of magnitude larger than E_1 .

V_3 displays more interesting behavior. Its trace in the three-boson sector is not fixed,

only the trace of $V_2 + V_3$ is fixed. The trace of V_2 in the three-boson sector varies because of its evolution in the two-boson sector, so the trace of V_3 varies to restore unitarity. Here we see $\langle\beta|V_{3s}|\beta\rangle$ becoming much greater than $\langle\alpha|V_{3s}|\alpha\rangle$ for both weak and strong coupling, because $\langle\beta|V_{3s}|\beta\rangle$ is fed by a term second-order in V_2 , which we will identify with a tree diagram in the next section.

For $g = -0.1$, $\langle\beta|V_{3s}|\beta\rangle$ grows to $\mathcal{O}(g^2)$ while $\langle\alpha|V_{3s}|\alpha\rangle$ only grows to $\mathcal{O}(g^3)$. $\langle\alpha|V_{3s}|\beta\rangle$ is initially comparable to $\langle\beta|V_{3s}|\beta\rangle$ because it is also fed by an $\mathcal{O}(V_2^2)$ tree-level interaction, but it is then driven exponentially to zero with all off-diagonal matrix elements. Additional features of this flow will be discussed in the next section.

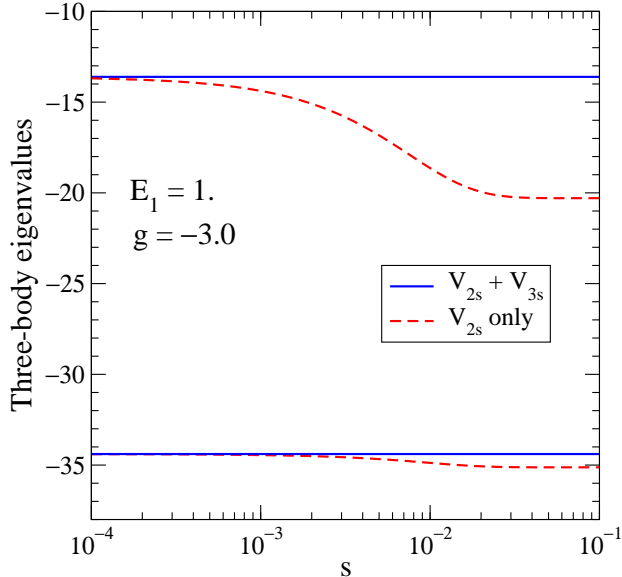


FIG. 3: The two lowest eigenvalues of the three-boson systems as a function of s with the full interaction and when the three-body interaction is omitted.

One measure of the importance of V_{3s} is the relative error in the three-boson eigenvalues when V_{3s} is not included; the errors arise because V_{2s} alone can not produce unitary flow in the three-boson sector. The eigenvalues for these two cases using $g = -3.0$ are shown in fig. 3. The eigenvalues are constant when the full interaction is included (“It’s unitary!”), while omitting V_{3s} leads to a small error for the ground state and a 50% error for the excited state. These errors are consistent with the missing matrix elements, $\langle\alpha|V_{3s}|\alpha\rangle$ and $\langle\beta|V_{3s}|\beta\rangle$, shown in fig. 2. For $g = -0.1$ the errors are too small to be easily visible.

Of course, there is no reason to restrict the initial hamiltonian to include two-body interactions alone. The unitary flow of V_{2s} is not altered if we add an initial three-body interaction, but that of V_{3s} can be altered drastically. None of the flow equations derived above change, only the initial values of V_3 matrix elements change. Off-diagonal matrix elements are still driven to zero and diagonal matrix elements yield the correct eigenvalues.

We illustrate how a three-body force added from the start affects unitary renormalization group evolution using another zero-range initial interaction:

$$V_3(x_i, x_j, x_k) = (2L)^2 g_3 \delta(x_i - x_j) \delta(x_j - x_k). \quad (36)$$

The initial matrix elements we need are $\langle\alpha|V_{3s}|\alpha\rangle = 10g_3$, $\langle\beta|V_{3s}|\beta\rangle = 6g_3$ and $\langle\alpha|V_{3s}|\beta\rangle = 5g_3$. Note the relatively large prefactors.

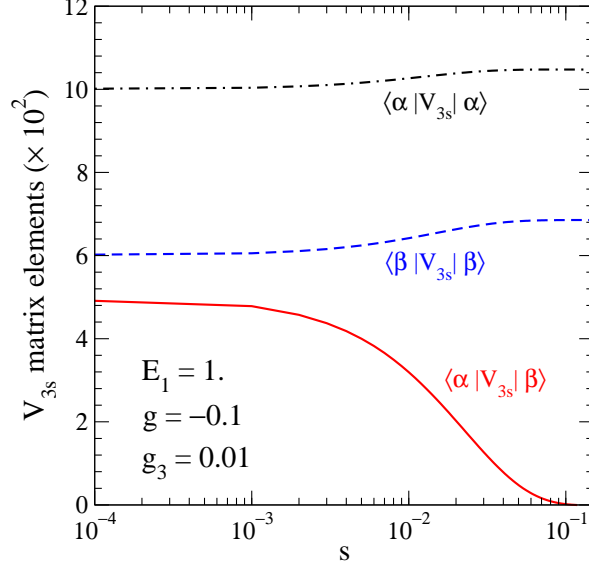


FIG. 4: Hamiltonian matrix elements of V_3 as a function of the flow parameter s in the three-boson sector for weak coupling, $g = -0.1$ and $g_3 = 0.01$.

In fig. 4 we display typical perturbative evolution, choosing $g = -0.1$ and $g_3 = 0.01$ so that V_2 and V_3 have comparable perturbative effects. The dominant effect of the perturbative three-body force is to both shift and split the three-boson energies. The off-diagonal matrix element decays exponentially to zero with little additional effect on the energies.

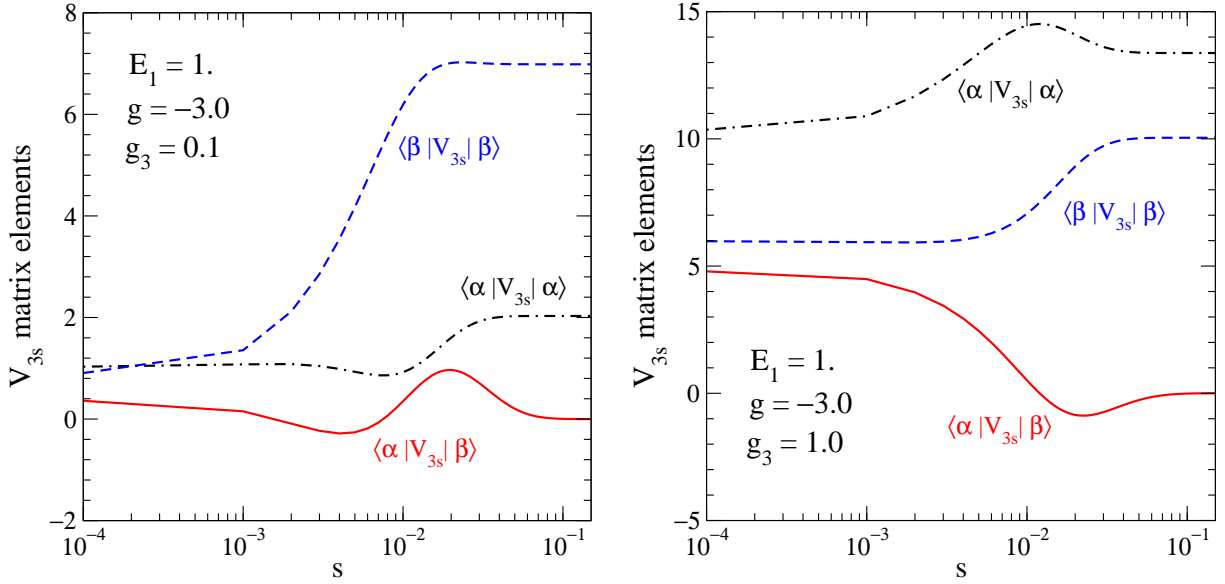


FIG. 5: Hamiltonian matrix elements of V_3 as a function of the flow parameter s in the three-boson sector for two sets of strong couplings.

In fig. 5 we display two examples of non-perturbative evolution, both with $g = -3.0$ as considered above, with $g_3 = 0.1$ an example where V_2 dominates the evolution and $g_3 = 1.0$ an example where V_3 dominates in the three-boson sector. These should be contrasted with

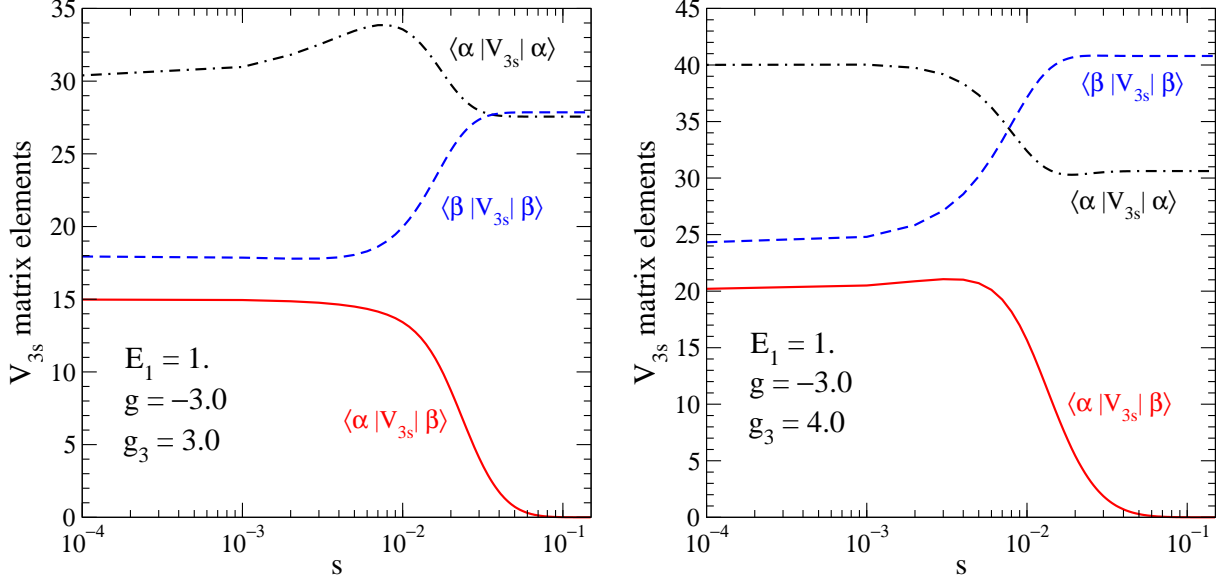


FIG. 6: Hamiltonian matrix elements of V_3 as a function of the flow parameter s in the three-boson sector for two additional sets of strong couplings.

fig. 2 in which $g_3 = 0$. Perhaps the most interesting feature to emerge as g_3 increases is that V_3 splits the three-boson energies with a different sign for intermediate values of g_3 . Figure 6 shows that as g_3 is further increased, the order of its three-boson splittings reverts to the perturbative ordering. This simple model actually displays a remarkably broad range of interesting, analytically understandable behavior as a function of the two couplings and our examples are not exhaustive.

IV. FOCK SPACE DIAGRAMMATIC ANALYSIS

While it is straightforward to generate coupled evolution equations for many-body interactions by computing explicit matrix elements of the operator evolution equations, this requires inserting a complete set of N -boson states to determine V_N and does not immediately expose disconnected interactions in which spectators do not participate. If one seeks a numerically tractable differential equation for the evolution of V_N in momentum representation, these disconnected matrix elements are best avoided because they contain momentum delta-functions for the spectator states. One of the advantages of a diagrammatic analysis is that it isolates these matrix elements as disconnected diagrams, which are exactly cancelled as long as V_{N-1} is fixed by solving the SRG equations in sectors with fewer than N particles.

We want to develop simple diagrammatic representations of $[[T, V], T + V]$, to generate explicit unitary flow equations for matrix elements of V . We must choose which many-boson matrix elements to represent. The matrix elements that immediately lead to simple diagrammatic rules are symmetrized, but not normalized for states containing more than one boson in a given mode. Since we use the same states on both sides of the unitary flow equation, normalization does not matter until we compute the explicit hamiltonian.

Eigenstates of T define particle creation and annihilation operators, $|n\rangle = a_n^\dagger|0\rangle$, with

$[a_m, a_n^\dagger] = \delta_{mn}$, in terms of which,

$$|i, j, k, \dots\rangle \equiv a_i^\dagger a_j^\dagger a_k^\dagger \cdots |0\rangle, \quad (37)$$

where i, j, k, \dots label external and internal legs in the diagrams. We associate an eigenvalue of T , E_i , with any line labelled by i . For two modes,

$$T = E_1 a_1^\dagger a_1 + E_2 a_2^\dagger a_2, \quad (38)$$

and for any number of modes,

$$T = \sum_i E_i a_i^\dagger a_i. \quad (39)$$

V_2 is then specified by $\{ij|V_2|kl\}$ and V_3 is specified by $\{ijk|V_3|lmn\}$:

$$V_2 = \left(\frac{1}{2!}\right)^2 \sum_{ijkl} a_i^\dagger a_j^\dagger \{ij|V_2|kl\} a_l a_k, \quad (40)$$

$$V_3 = \left(\frac{1}{3!}\right)^2 \sum_{ijklmn} a_i^\dagger a_j^\dagger a_k^\dagger \{ijk|V_3|lmn\} a_n a_m a_l. \quad (41)$$

In our simple example above, these indices took on only the values 1 and 2, but this constraint does not simplify the diagrammatic rules and we need impose it only at the end to verify that the rules produce the same equations as derived in the previous section.

We are now in a position to develop a complete set of diagrammatic rules for the right-hand-side of the flow equations for $\{ij|V_2|kl\}$ and $\{ijk|V_3|lmn\}$. In fig. 7 we show a diagrammatic representation for the basic elements of these flow equations. All terms are built from V_N , $\overline{V}_N \equiv [T, V_N]$ and $\overline{\overline{V}}_N \equiv [[T, V_N], T]$, where $\{ij|\overline{V}_2|kl\} = (E_i + E_j - E_k - E_l)\{ij|V_2|kl\}$, and similar relations are easily found for all matrix elements of \overline{V}_N and $\overline{\overline{V}}_N$. External legs on these diagrams are labeled with symmetrized labels, so we will not count diagrams as “topologically distinct” if they result from a permutation of indices associated with the legs of a single vertex. The redundancies from these permutations cancel the $(1/2!)^2$ in V_2 and the $(1/3!)^2$ in V_3 , except in diagrams with loops, where an N -loop diagram is weighted by $1/(N+1)!$. Diagrams with one loop are assigned a factor of $1/2$, etc.

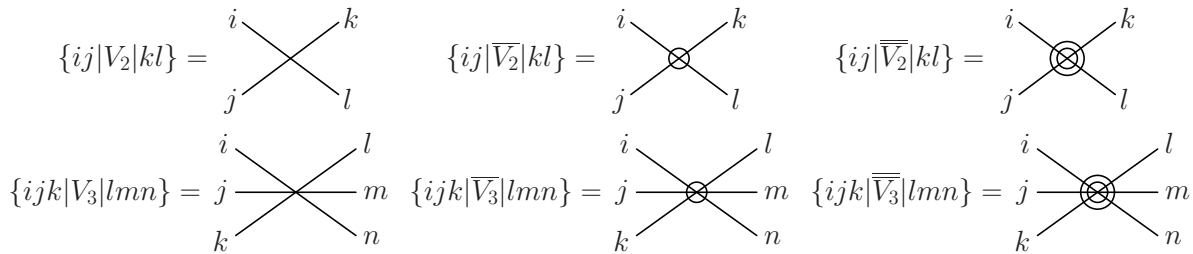


FIG. 7: Labelled vertices represent matrix elements of V_N , $\overline{V}_N \equiv [T, V_N]$, and $\overline{\overline{V}}_N \equiv [[T, V_N], T]$.

In fig. 8 we show a schematic representation of the diagrams that appear in the SRG flow equations in the two-boson and three-boson sectors. Diagrammatic rules are easily deduced

$$\begin{aligned}
\frac{dV_2}{ds} &= \text{Diagram 1} + \text{Diagram 2} - \text{Diagram 3} \\
\frac{dV_3}{ds} &= \text{Diagram 4} + \text{Diagram 5} + \text{Diagram 6} + \text{Diagram 7} + \dots
\end{aligned}$$

FIG. 8: Complete diagrammatic representation of dV_2/ds and a schematic representation of the diagrams for dV_3/ds . For the latter, there are eighteen tree diagrams, six one-loop diagrams, and two two-loop diagrams.

from the equations and are readily generalized to any sector. For clarity we expand eq. (21):

$$\begin{aligned}
\frac{dV_{2s}}{ds} + \frac{dV_{3s}}{ds} &= [[T, V_{2s}], T] + [[T, V_{3s}], T] \\
&\quad + [[T, V_{2s}], V_{2s}] + [[T, V_{2s}], V_{3s}] + [[T, V_{3s}], V_{2s}] + [[T, V_{3s}], V_{3s}] \\
&= \overline{\overline{V}}_2 + \overline{\overline{V}}_3 + \left\{ \left([\overline{V}_2, V_2] + [\overline{V}_2, V_3] + [\overline{V}_3, V_2] + [\overline{V}_3, V_3] \right) \right. \\
&\quad \left. - \left(V_2 \leftrightarrow \overline{V}_2, V_3 \leftrightarrow \overline{V}_3 \right) \right\}. \tag{42}
\end{aligned}$$

Diagrams represent symmetrized matrix elements of these equations. Every line carries a label and products of \overline{V} and V result in contractions that equate indices on lines between the two vertices. Once indices are assigned to all lines, vertices represent matrix elements of V_2 , V_3 , \overline{V}_2 and \overline{V}_3 , with indices matched to lines. There is a sum over all internal indices, so even tree diagrams represent sums. One-loop diagrams appear in the evolution of V_2 , while both one- and two-loop diagrams govern the evolution of V_3 . In general, tree diagrams through $(N - 1)$ -loop diagrams appear in the evolution of V_N .

The structure of eq. (42) guarantees that V_{2s} is completely determined by two-boson matrix elements, with V_{3s} then determined by three-boson matrix elements. Comparing eq. (42) with fig. 8, note that V_2 and V_3 appear together in the equation but there are separate diagrammatic equations for their evolution. Two-boson matrix elements of eq. (42) produce the diagrammatic equation for dV_2/ds , while three-boson matrix elements produce the diagrammatic equation for dV_3/ds . When three-boson matrix elements of eq. (42) are computed, the matrix elements of dV_2/ds on the left-hand-side cancel against diagrams on the right-hand-side that are identical to the two-boson diagrams with a spectator line that is not connected to either vertex. As long as dV_2/ds solves the two-boson evolution equations, these disconnected diagrams can be dropped on the right-hand-side of the diagrammatic equation and only dV_3/ds appears on the left-hand-side.

There are two reasons that disconnected diagrams never appear. Diagrams in which both vertices are not connected to one another by at least one line vanish because of the commutator structure, $[\overline{V}, V]$. If there are no contractions between creation and annihilation operators in these two vertices, the two terms from the commutator produce identical matrix elements that exactly cancel.

As discussed above, diagrams in which an external line is not connected to any vertex, such as three-boson diagrams in which a single spectator line appears with the one-loop interactions between the other two bosons as displayed below in fig. 9, simply produce copies of the flow equations from lower sectors of Fock space. So, if V_2 satisfies the two-boson flow equations, disconnected three-boson matrix elements of dV_2/ds cancel the disconnected matrix elements of $[\overline{V}_2, V_2]$. We isolate the flow equation for dV_3/ds simply by dropping these disconnected diagrams and setting dV_3/ds equal to the sum of connected diagrams, including the diagram for $\overline{\overline{V}}_3$.

So, V_2 is determined by two-boson matrix elements, because V_3 , V_4 , etc. will not appear in this sector and all diagrams that do appear in the two-boson sector also appear in the three-boson sector with one disconnected line, in the four-boson sector with two disconnected lines, etc. Again, if V_2 satisfies the flow equation in the two-boson sector, no disconnected diagrams survive in the flow equation for V_3 in the three-boson sector. In the three-boson sector, there are tree diagrams involving two powers of V_2 , one-loop diagrams involving one power of V_2 and one power of V_3 , and two-loop diagrams involving two powers of V_3 . V_2 is already determined by the two-boson evolution equation and V_3 is the only new interaction appearing in the three-boson evolution equations, so the three-boson evolution equations determine V_3 .

This type of analysis is easily generalized to higher sectors because of the simple second-order structure of the exact unitary flow equation. V_4 is determined by the four-boson evolution equations. These include tree-diagrams with one power of V_2 and one of V_3 , one-loop diagrams with one power of V_2 and one power of V_4 or with two powers of V_3 , two-loop diagrams with one power of V_3 and one power of V_4 , and three-loop diagrams that are second-order in V_4 .

$$\frac{d}{ds}\{ij|V_2|kl\} = \text{tree diagram} + \text{one-loop diagram} - \text{one-loop diagram}$$

FIG. 9: Diagrammatic representation of eq. (43).

In fig. 9 the complete set of labelled two-boson diagrams is shown, from which we obtain

$$\frac{d}{ds}\{ij|V_2|kl\} = \{ij|\overline{\overline{V}}_2|kl\} + \frac{1}{2!} \sum_{mn} (\{ij|\overline{V}_2|mn\}\{mn|V_2|kl\} - \{ij|V_2|mn\}\{mn|\overline{V}_2|kl\}) . \quad (43)$$

Substituting for \overline{V}_2 and $\overline{\overline{V}}_2$ we find

$$\frac{d}{ds}\{ij|V_2|kl\} = -(E_{ij} - E_{kl})^2 \{ij|V_2|kl\} + \frac{1}{2!} \sum_{mn} (E_{ij} + E_{kl} - 2E_{mn}) \{ij|V_2|mn\}\{mn|V_2|kl\} , \quad (44)$$

where $E_{ij} = E_i + E_j$. It is straightforward to show that when sums are restricted to the lowest two modes, eqs. (22)–(24) are reproduced.

In fig. 10 the complete set of labelled three-boson diagrams is shown. This equation is for the evolution of V_3 , with V_2 solving the two-boson equations above and no disconnected diagrams appearing as a result. There are eighteen distinct tree-level diagrams, twelve one-loop diagrams and two two-loop diagrams. We do not explicitly display all possible external

$$\begin{aligned}
\frac{d}{ds}\{ijk|V_3|lmn\} = & \begin{array}{c} i \quad l \\ \diagdown \quad \diagup \\ j \text{---} \bigcirc \text{---} m \\ \diagup \quad \diagdown \\ k \quad n \end{array} + \begin{array}{c} i \quad l \\ \diagdown \quad \diagup \\ j \text{---} \bigcirc \text{---} m \\ \diagup \quad \diagdown \\ k \quad n \end{array} - \begin{array}{c} i \quad l \\ \diagdown \quad \diagup \\ j \text{---} \bigcirc \text{---} m \\ \diagup \quad \diagdown \\ k \quad n \end{array} \\
& + 8 \, i, j \leftrightarrow k \text{ and } m, n \leftrightarrow l \text{ permutations} \\
& + \begin{array}{c} i \quad l \\ \diagdown \quad \diagup \\ j \text{---} \bigcirc \text{---} m \\ \diagup \quad \diagdown \\ k \quad n \end{array} - \begin{array}{c} i \quad l \\ \diagdown \quad \diagup \\ j \text{---} \bigcirc \text{---} m \\ \diagup \quad \diagdown \\ k \quad n \end{array} \\
& + 2 \, i, j \leftrightarrow k \text{ permutations} \\
& + \begin{array}{c} i \quad l \\ \diagdown \quad \diagup \\ j \text{---} \bigcirc \text{---} m \\ \diagup \quad \diagdown \\ k \quad n \end{array} - \begin{array}{c} i \quad l \\ \diagdown \quad \diagup \\ j \text{---} \bigcirc \text{---} m \\ \diagup \quad \diagdown \\ k \quad n \end{array} \\
& + 2 \, m, n \leftrightarrow l \text{ permutations} \\
& + \begin{array}{c} i \quad l \\ \diagdown \quad \diagup \\ j \text{---} \bigcirc \text{---} m \\ \diagup \quad \diagdown \\ k \quad n \end{array} - \begin{array}{c} i \quad l \\ \diagdown \quad \diagup \\ j \text{---} \bigcirc \text{---} m \\ \diagup \quad \diagdown \\ k \quad n \end{array}
\end{aligned}$$

FIG. 10: Diagrammatic representation of eq. (45). The notation $i, j \leftrightarrow k$ means $i \leftrightarrow j$ or $j \leftrightarrow k$.

legs in the diagrams or the equations but list them as permutations. The resulting equation is

$$\begin{aligned}
\frac{d}{ds}\{ijk|V_3|lmn\} = & \{ijk|\overline{V}_3|lmn\} \\
& + \sum_p (\{ij|\overline{V}_2|lp\}\{pk|V_2|mn\} - \{ij|V_2|lp\}\{pk|\overline{V}_2|mn\} \\
& \quad + 8 \, i, j \leftrightarrow k, \, m, n \leftrightarrow l \text{ permutations}) \\
& + \frac{1}{2!} \sum_{pq} (\{ij|\overline{V}_2|pq\}\{pqk|V_3|lmn\} - \{ij|V_2|pq\}\{pqk|\overline{V}_3|lmn\} \\
& \quad + 2 \, i, j \leftrightarrow k \text{ permutations}) \\
& + \frac{1}{2!} \sum_{pq} (\{ijk|\overline{V}_3|lpq\}\{pq|V_2|mn\} - \{ijk|V_3|lpq\}\{pq|\overline{V}_2|mn\} \\
& \quad + 2 \, m, n \leftrightarrow l \text{ permutations}) \\
& + \frac{1}{3!} \sum_{pqr} (\{ijk|\overline{V}_3|pqr\}\{pqr|V_3|lmn\} - \{ijk|V_3|pqr\}\{pqr|\overline{V}_3|lmn\}) . \quad (45)
\end{aligned}$$

Most of the terms on the right-hand-sides of these equations are given by permutations of the indices in the terms explicitly displayed. For example, in the tree diagrams in fig. 10, one particle line on the left is connected to a different vertex than the other two. We must explicitly add each permutation of the index assigned to this line, obtaining additional diagrams in which this index is i instead of k and j instead of k . Permutations of the two lines connected to the same vertex are considered “topologically identical” to the diagram

shown, so they produce no new diagrams. This reflects the fact that $\{ij|V_2|pq\} = \{ji|V_2|pq\}$.

In front of each sum over N indices there is a factor $1/N!$, so to each N -loop diagram we associate this factor of $1/N!$. These sums are unrestricted; if we replace them with sums over distinct permutations the factor of $1/N!$ drops out.

It is again a straightforward but tedious exercise to show that truncation to the two lowest modes yields eqs. (31)–(33). To match equations, note that $|a\rangle = \sqrt{1/2} |11\rangle$, $|b\rangle = \sqrt{1/2} |22\rangle$ and $|c\rangle = |12\rangle$ are the two-boson states we need, while $|\alpha\rangle = \sqrt{1/6} |111\rangle$ and $|\beta\rangle = \sqrt{1/2} |122\rangle$ are the only positive parity three-boson states we need.

If the hamiltonian has no three-body force at the start of SRG evolution, one will be produced. Initially, the tree diagrams, which are second-order in V_2 , dominate. Next $\overline{\overline{V}}_3$ will suppress far off-diagonal matrix elements while terms of order V_2V_3 will be more important near the diagonal, with the two-loop diagram emerging last since it is order V_3^2 . Naturally, if V_3 is not zero at the start of the renormalization group evolution, the relative magnitude of these contributions can change. The diagrams provide a tool for analyzing various contributions to the flow equations and seeking approximations, which might be essential in more realistic calculations.

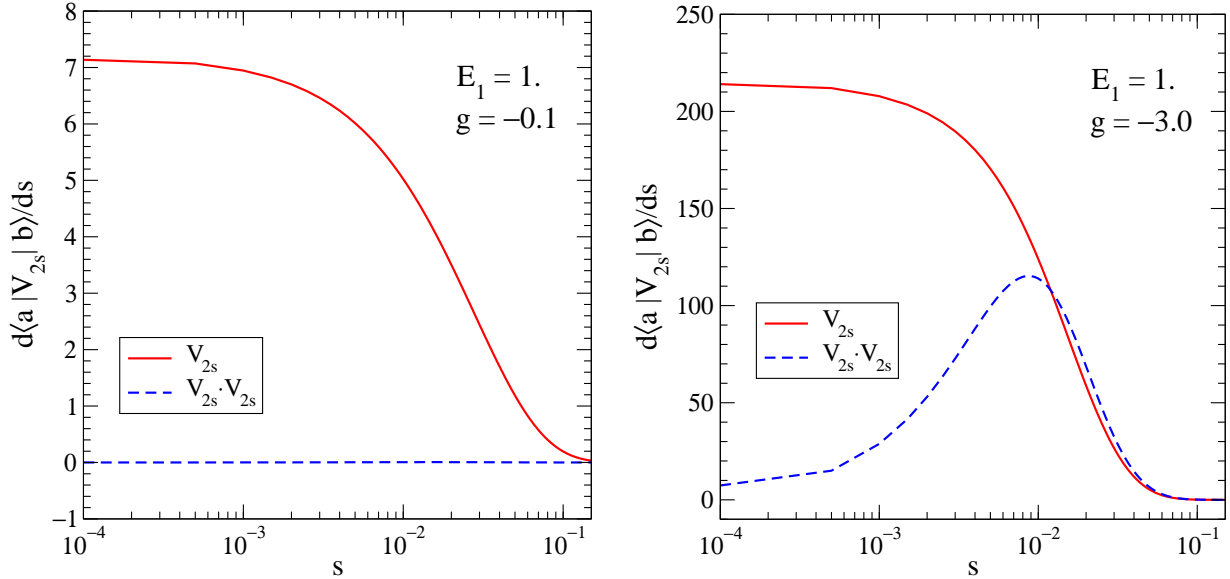


FIG. 11: Matrix elements that contribute to $\frac{d}{ds}\langle a|V_{2s}|b\rangle$ in the two-boson sector for weak and strong coupling. $\langle a|V_{2s}|b\rangle$ is dominated by $\overline{\overline{V}}_2$, with the second-order one-loop correction barely visible when $g = -0.1$.

In figs. 11–15 we contrast various contributions to the evolution of V_2 and V_3 for weak coupling, $g = -0.1$, and strong coupling, $g = -3.0$. Figure 11 displays contributions to the off-diagonal matrix element $\langle a|V_{2s}|b\rangle$. In both cases the initial evolution is dominated by the double-commutator, $\overline{\overline{V}}_2$, which always drives off-diagonal matrix elements to zero exponentially. For weak coupling the one-loop, $\mathcal{O}(V_2^2)$, contribution remains negligible throughout the evolution, while for strong coupling it becomes comparable to that of $\overline{\overline{V}}_2$ and helps drive $\langle a|V_{2s}|b\rangle$ to zero. This qualitative behavior is what is seen when this transformation is applied to realistic nucleon-nucleon interactions [2, 3], but it is possible to find cases where the one-loop contribution first opposes $\overline{\overline{V}}_2$ and forces $\langle a|V_{2s}|b\rangle$ to grow before $\overline{\overline{V}}_2$ finally takes

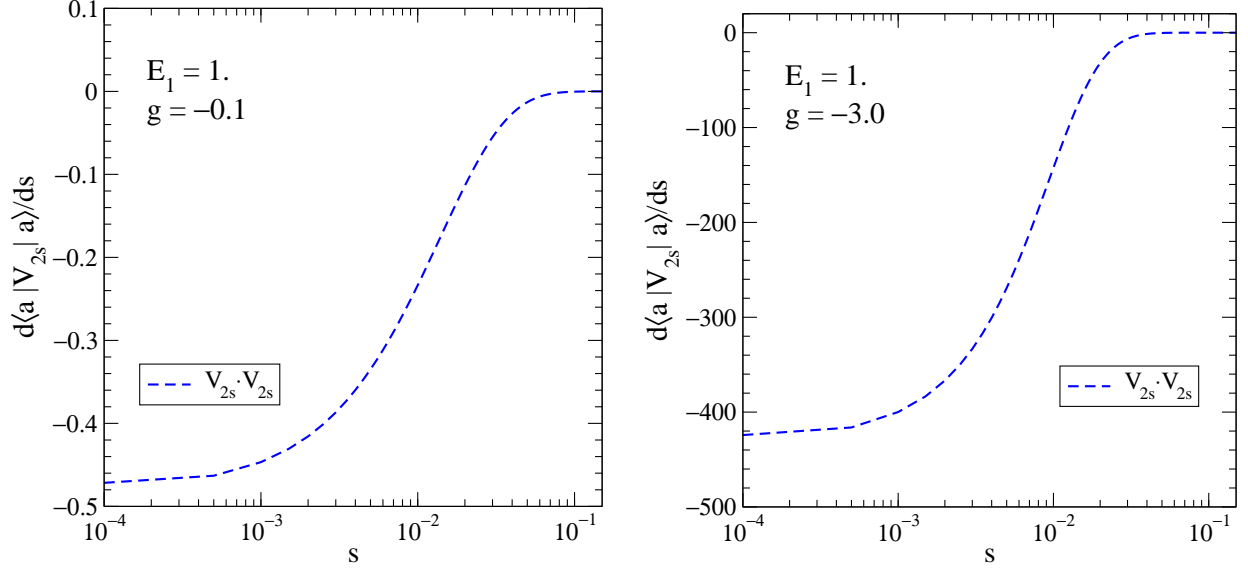


FIG. 12: Matrix elements that contribute to $\frac{d}{ds}\langle a|V_{2s}|a\rangle$ in the two-boson sector for weak and strong coupling. Only the one-loop diagram contributes.

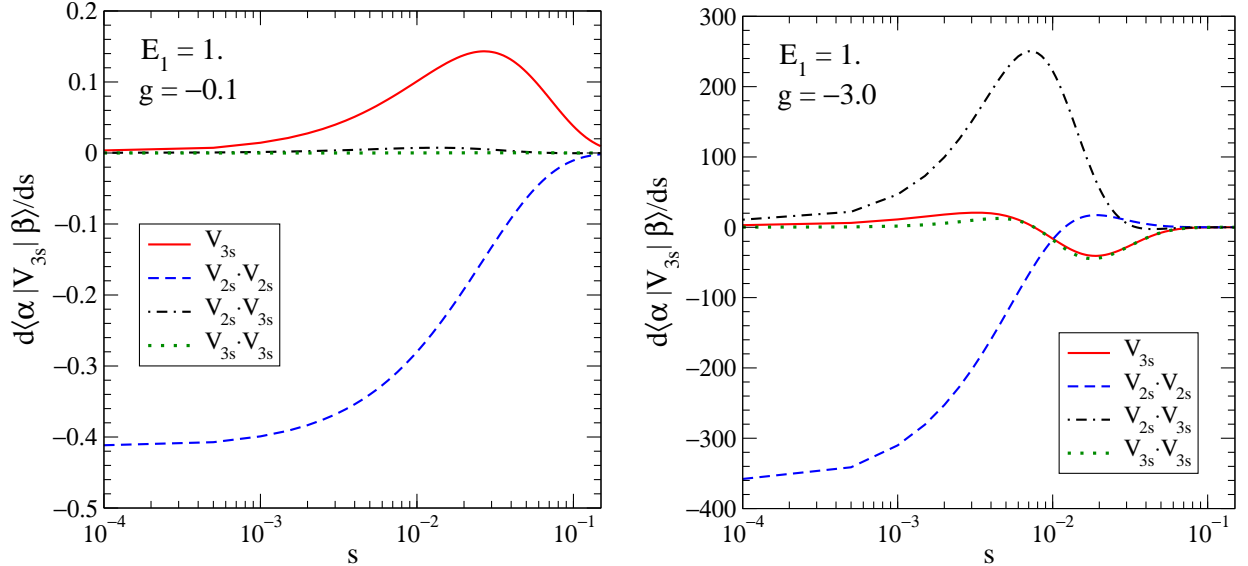


FIG. 13: Matrix elements that contribute to $\frac{d}{ds}\langle \alpha|V_{3s}|\beta\rangle$ in the three-boson sector for weak and strong coupling. Tree diagrams initially dominate the evolution of $\langle \alpha|V_{3s}|\beta\rangle$, allowing \overline{V}_3 to grow and then drive $\langle \alpha|V_{3s}|\beta\rangle$ to zero. Here again, the one-loop and two-loop contributions are barely visible for $g = -0.1$ and the two-loop contribution remains negligible even for strong coupling. This can change if V_3 is not zero initially.

over [9]. This happens when the running cutoff encounters a bound state threshold and we make no attempt to discuss such interesting exceptions in this paper, although they are inevitable in three-body systems that display the Efimov effect [10, 11].

Figure 12 shows the sole one-loop contribution to the evolution of the diagonal matrix element $\langle a|V_{2s}|a\rangle$. Since the trace of H_s is conserved in each sector of Fock space, contributions

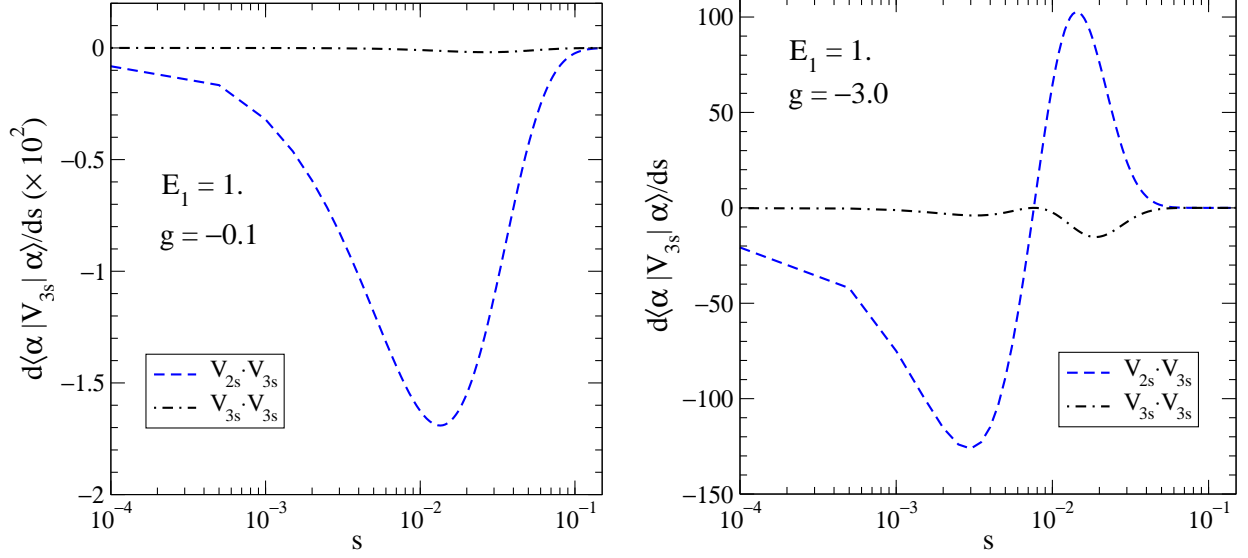


FIG. 14: Matrix elements that contribute to $\frac{d}{ds}\langle\alpha|V_{3s}|\alpha\rangle$ in the three-boson sector for weak and strong coupling. No tree diagrams contribute to $\langle\alpha|V_{3s}|\alpha\rangle$, and the relatively small one-loop contributions dominate over the two-loop contributions in both cases.

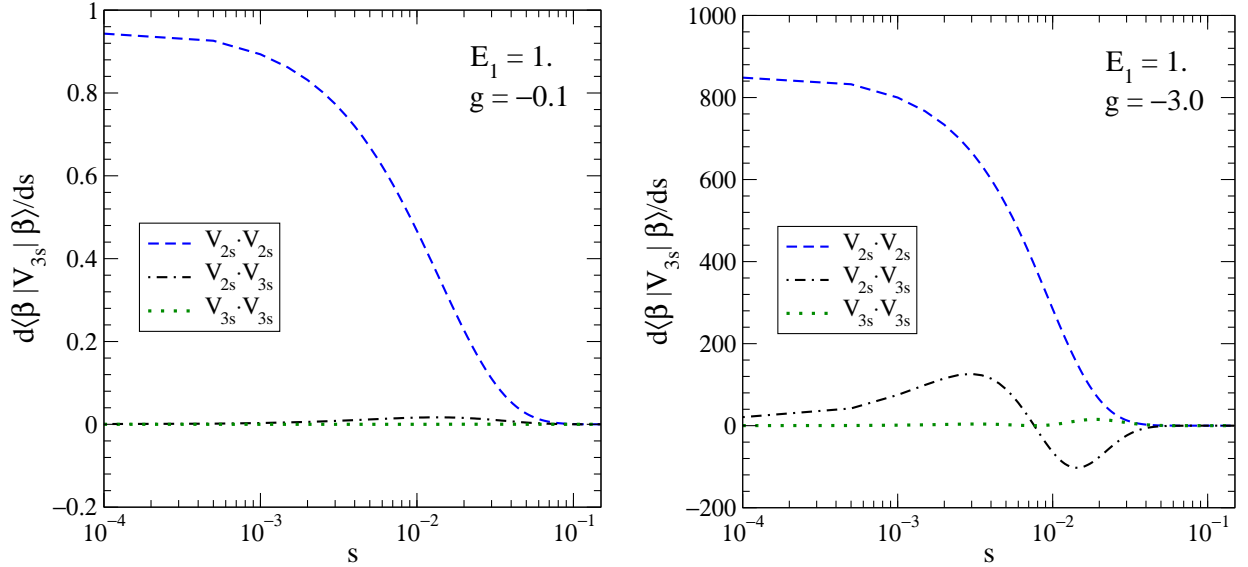


FIG. 15: Matrix elements that contribute to $\frac{d}{ds}\langle\beta|V_{3s}|\beta\rangle$ in the three-boson sector for weak and strong coupling. Tree diagrams dominate the initial evolution of $\langle\beta|V_{3s}|\beta\rangle$, with relatively small one-loop contributions and negligible two-loop contributions in both cases.

to $\langle b|V_{2s}|b\rangle$ simply have the opposite sign. The only change from weak to strong coupling is the magnitude of the one-loop contribution. This simplicity is partially a reflection of the drastic truncation of Fock space but a similar exponential fall-off in strength is guaranteed in more realistic examples as long as the transformation drives the matrix to band-diagonal form. Not only do the far off-diagonal matrix elements flow to zero exponentially, the diagonal matrix elements evolve rapidly at first and then slow as they approach their asymptotic values. Again, there are exceptions to this simple evolution if bound-state thresholds are

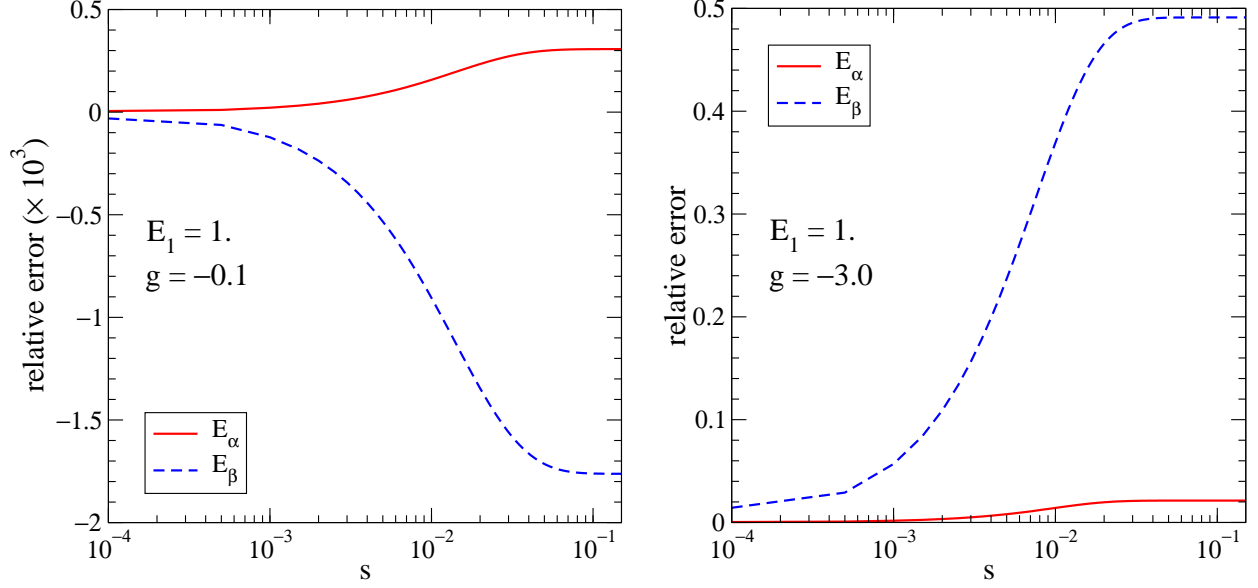


FIG. 16: Relative errors in the three-boson eigenvalues for weak and strong coupling when V_3 is simply dropped.

encountered [9].

In figs. 13–15 we turn to terms that contribute to the evolution of V_3 . In fig. 13 we immediately see that tree diagrams, which are $\mathcal{O}(V_2^2)$, dominate the initial evolution of $\langle \alpha | V_{3s} | \beta \rangle$ for both weak and strong coupling. This is guaranteed when V_3 itself starts at zero, but the subsequent evolution differs for weak and strong coupling. For weak coupling, once $\langle \alpha | V_{3s} | \beta \rangle$ itself has any appreciable strength, $\overline{\overline{V}}_3$ builds and drives this off-diagonal matrix element back to zero. One-loop and two-loop contributions remain negligible for all s when the coupling is weak, simply because these terms are suppressed by powers of g . At strong coupling it is the one-loop contribution that builds to shut off the growth of $\langle \alpha | V_{3s} | \beta \rangle$ and then drive it to zero, while $\overline{\overline{V}}_3$ and the two-loop contribution remain small but non-negligible near the end of the evolution.

The evolution of $\langle \alpha | V_{3s} | \alpha \rangle$ and $\langle \beta | V_{3s} | \beta \rangle$ are not simply connected by a trace constraint because V_2 also contributes to the trace of H_s in the three-boson sector. There is no tree diagram contributing to $\langle \alpha | V_{3s} | \alpha \rangle$, so it remains small in comparison to $\langle \beta | V_{3s} | \beta \rangle$ for both weak and strong coupling. We see in fig. 14 that the one-loop diagram dominates for both weak and strong coupling, but this contribution changes sign during the evolution of $\langle \alpha | V_{3s} | \alpha \rangle$ for strong coupling. Figure 15 shows that the tree diagram dominates this evolution, with other contributions remaining negligible throughout the evolution at weak coupling and only the one-loop contribution becoming significant at strong coupling.

In fig. 16 we show the fractional error in the three-boson eigenvalues E_α and E_β when V_3 is simply dropped. This error remains smaller than $\mathcal{O}(g^2)$ for weak coupling, which is the order of the tree diagrams that are ignored, and grows to 50% for strong coupling. In both cases it is E_β that is most sensitive to V_3 .

In fig. 17 we show these same fractional errors after approximating V_3 by evolving with only the tree diagrams and $\overline{\overline{V}}_3$. This significantly reduces the errors in E_β from simply dropping V_3 for both weak and strong coupling. This is consistent with the observations above about the small relative strength of the one-loop and two-loop contributions. Finally,

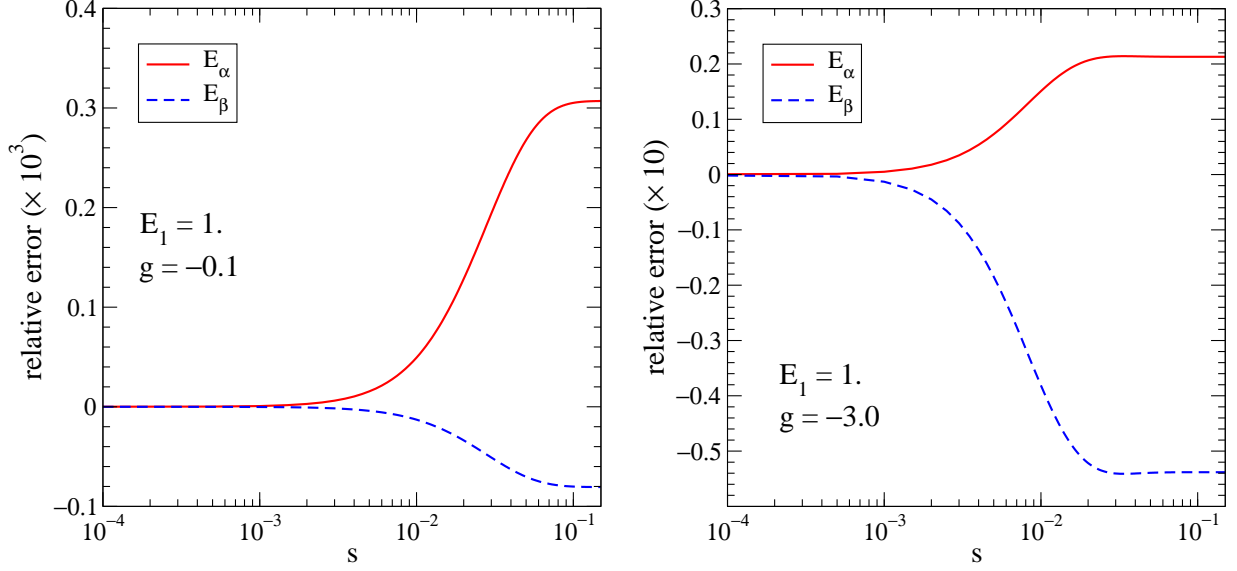


FIG. 17: Relative errors in the three-boson eigenvalues for weak and coupling when $\overline{\overline{V}}_3$ and tree diagrams are used to evolve V_3 .

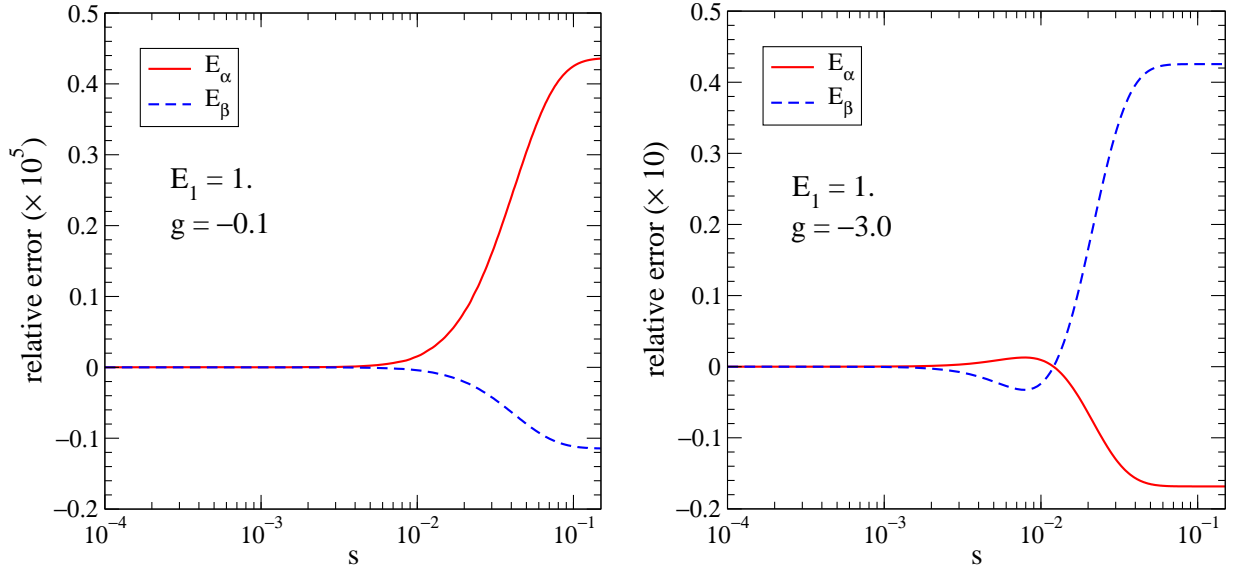


FIG. 18: Relative errors in the three-boson eigenvalues for weak and strong coupling when tree and one-loop diagrams are used to evolve V_3 .

in fig. 18 we show these errors when V_3 is evolved using both tree and one-loop diagrams, dropping only the two-loop diagrams. This further reduces the errors for weak coupling but not for strong coupling, where we have seen in fig. 13 that the two-loop contribution, although smaller than the one-loop contribution, becomes comparable to the contribution of $\overline{\overline{V}}_3$ throughout the evolution.

It should be clear that this analysis is easily extended to the four-boson sector, where V_4 must be added. For weak coupling, we should again find that tree diagrams which are $\mathcal{O}(V_2 V_3)$ will dominate in the evolution of V_4 . Since there are no diagrams contributing to

V_4 built only from two powers of V_2 , V_4 is fed entirely by induced interactions and might remain small even for strong two-body interactions, but explicit calculations are required to find what happens at strong coupling.

V. SUMMARY

In this paper, we have used a simple two-level model system to illustrate how a unitary SRG consistently evolves two-body and three-body interactions. We have developed a diagrammatic treatment of the SRG equations that applies generally and have shown how it can be used with a variety of examples in our model. However, such a model might seem too schematic to offer insight into realistic problems. In fact, the steps to the physics problem that originally motivated this work, that of describing atomic nuclei from microscopic interactions, are not so large.

The low-energy nuclear many-body problem has been one of the most important problems in physics for over seventy years, but it has stubbornly resisted a complete solution. In recent years, however, it has become clear that a Wilsonian renormalization group perspective leads to new conceptual and practical ways to attack this problem. The primary tool Wilson introduced to renormalization group formalism is a renormalization transformation that lowers a well-defined hamiltonian resolution, a tool that is ideally suited to finding universal interactions. Feed any interaction constrained by low-energy data into a well-designed RG transformation, it produces a universal low-energy interaction that is decoupled from the ambiguous (and irrelevant) high-energy components of the input interaction.

The same RG transformation that Wilson employed in his first non-perturbative RG calculation [12] has recently been applied to a wide variety of modern nucleon-nucleon interactions [13, 14] and every one of them was transformed into a nearly universal low-energy effective nucleon-nucleon interaction, called $V_{\text{low } k}$. It turns out that $V_{\text{low } k}$ also drastically reduces the complexity of the nuclear many-body problem but requires the consistent evolution of three-nucleon interactions [16].

Realistic nucleon-nucleon (NN) interactions include strong short-range repulsion and a strong tensor force. These lead to far off-diagonal strength in the momentum representation of the nucleon-nucleon interaction, so that large matrices are required to represent this interaction. The size of these matrices increases rapidly with particle number. $V_{\text{low } k}$ requires drastically fewer matrix elements to accurately reproduce all low-energy NN scattering data, and this reduction exponentiates as we move to the many-nucleon problem [7]. In contrast to conventional NN interactions, which are highly nonperturbative, $V_{\text{low } k}$ leads to nearly converged nuclear matter calculations at second order in many-body perturbation theory. The three-nucleon interaction is an essential ingredient in saturating nuclear matter close to the empirical density and binding energy [15]. Even more, the problem is not well-posed until consistent few-body interactions are found, as the nucleon-nucleon interaction on its own does not maintain unitarity in even the three-nucleon problem and violations are comparable to nuclear level spacings [7].

The SRG transformation we employ produces basically the same universal nucleon-nucleon interaction as the $V_{\text{low } k}$ evolution and shares the same positive features. Perhaps the most important advantage of the type of SRG transformation used here is that it “automatically” allows us to consistently evolve two- and few-nucleon interactions. Just as we have seen in our model, if the 3-body force is not included in the evolution, few-body observables are cutoff dependent and errors can be large. This article represents a first step towards the

computation of a fully consistent low-momentum three-nucleon interaction. In addition to the three-nucleon interaction that is required by unitarity when the two-nucleon interaction flows, there is an intrinsic three-nucleon interaction that must be added; current versions include various phenomenological and chiral effective field theory potentials. Ideally the SRG transformation will again reveal a universal low-momentum, three-nucleon interaction.

In principle, four-nucleon interactions can also be included and may be needed for quantitative nuclear structure, particularly for heavy nuclei. The three-loop diagrams in the SRG equations represent nine-dimensional integrals and the spin-isospin algebra also grows in complexity. But we have seen in our model that even for strong couplings we can sometimes accurately approximate the SRG evolution equations by dropping such multi-loop contributions and we may even obtain better than 10% accuracy using tree diagrams alone; 10% accuracy for an already small correction might be sufficient. There are no integrals in these tree diagrams, so we need “only” deal with the spin-isospin algebra for four nucleons. But this is idle speculation until the three-body interaction is computed accurately. With a three-nucleon interaction in hand we can directly test the importance of V_4 by studying violations of unitarity in ^4He , for example.

The basic procedure for evolving two-nucleon and three-nucleon interactions with a unitary RG transformation is the same as that illustrated in this article. The square well must be removed, bosons must be replaced by nucleons, one dimension goes to three dimensions and the initial hamiltonian must include realistic inter-nucleon interactions. Removing the square well and replacing bosons with fermions is uncomplicated, while moving up to three dimensions and using realistic interactions requires more work but no major conceptual developments.

It is important to realize that in nuclear calculations, we do not intend to use the transformation to diagonalize the hamiltonian as we have in this article. In realistic many-body problems we run the flow parameter s only to the point where low- and high-energy degrees of freedom are decoupled in the few-nucleon sectors. Running the transformation beyond this point would produce long-range few-body forces and strong many-body forces; we would effectively be forced to solve both few- and many-nucleon problems completely. We want to simplify the few-body forces that are then employed in many-nucleon calculations, not diagonalize the hamiltonian in every sector of Fock space and produce the large tower of many-body forces that would be required to do this in the many-body sectors. When we achieve sufficient decoupling in the two-nucleon sector, we compute the three-nucleon interaction using methods illustrated in this article and then switch to conventional few- or many-body methods using this partially diagonalized hamiltonian. See Refs. [2] and [3] for details.

Perhaps the most interesting immediate extension of the model we present is to remove the square well and let T simply be the kinetic energy. Instead of discrete sums, we obtain integrals over continuous momenta, but these can be approximated using a discrete mesh, so we once again have sums over discrete indices. N bosons interacting via a two-body delta-function potential in one dimension produce one bound state whose wave function and energy are known analytically [17]. Using momentum eigenstates we must compute the evolution of $\{k_1, k_2 \mid V_2 \mid k'_1, k'_2\}$ and $\{k_1, k_2, k_3 \mid V_3 \mid k'_1, k'_2, k'_3\}$. These can then be used in a numerical basis function calculation that should converge increasingly rapidly with basis size to the analytic result as the unitary transformation is run. With this discrete basis, the evolution equations are almost identical to those in this article.

The basic unitary renormalization group equation we employ in this article, eq. (5), is

the same in three dimensions as in one. Replacing bosons with fermions means only minor changes in the diagrammatic rules for the evolution equations, with the familiar minus signs from fermion exchange and no symmetry factors associated with loops. Exploiting angular momentum algebra and choosing appropriate Jacobi coordinates for three-nucleon states introduce technical complications, but these appear in a form almost identical to what is faced when solving three-nucleon Faddeev equations [18]. The SRG equations governing the evolution of the nuclear three-body force are only a scaled-up version (larger matrices) of our model problem, as opposed to the multi-channel complications of the Faddeev equations.

In this article we have chosen one simple operator for T , but there are many possible choices and this freedom can be exploited to improve convergence in many-body calculations. The calculations in this article are easily modified for any T that can be defined by diagonal matrix elements in the square well basis. T can itself depend on the flow parameter. Wegner [5] advocated using the diagonal matrix elements of H_s itself, which corresponds in the 2×2 matrix model to choosing $T = \omega_z(s)\sigma_z$. Wegner's transformation is guaranteed to drive the momentum representation of the hamiltonian to diagonal form, while other choices can produce divergent matrix elements and stall. These considerations are discussed in the context of simple models in Ref. [9].

Acknowledgments

We thank E. Anderson, S. Glazek, E. Jurgenson, and A. Schwenk for useful comments. This work was supported in part by the National Science Foundation under Grant Nos. PHY-0354916, PHY-0456903, and PHY-0653312 and by the UNEDF SciDAC Collaboration under DOE Grant DE-FC02-07ER41457.

-
- [1] K. G. Wilson, Adv. Math. **16** (1975) 170.
 - [2] S. K. Bogner, R. J. Furnstahl and R. J. Perry, Phys. Rev. C **75** (2007) 061001(R).
 - [3] S.K. Bogner, R.J. Furnstahl, R.J. Perry and A. Schwenk, Phys. Lett. B **649** (2007) 488.
 - [4] See <http://www.physics.ohio-state.edu/~ntg/srg/> for documentary examples.
 - [5] F. Wegner, Ann. Phys. (Leipzig) **3** (1994) 77.
 - [6] S.D. Glazek and K.G. Wilson, Phys. Rev. D **48** (1993) 5863; Phys. Rev. D **49** (1994) 4214.
 - [7] S.K. Bogner, R.J. Furnstahl, P. Maris, R.J. Perry, A. Schwenk and J.P. Vary, arXiv:0708.3754.
 - [8] S. Szpigel and R. J. Perry, in *Quantum Field Theory, A 20th Century Profile* ed. A.N. Mitra, (Hindustan Publishing Com., New Delhi, 2000), arXiv:hep-ph/0009071.
 - [9] S.D. Glazek and R.J. Perry, *The impact of bound states on similarity renormalization group transformations*; in preparation.
 - [10] V. Efimov, Phys. Lett. **33B**, 563 (1970).
 - [11] V. N. Efimov, Sov. J. Nucl. Phys. **12**, 589 (1971) [Yad. Fiz. **12**, 1080 (1970)].
 - [12] K. G. Wilson, Phys. Rev. **D2**, 1438 (1970).
 - [13] S. K. Bogner, T. T. S. Kuo and A. Schwenk, Phys. Rept. **386**, 1 (2003).
 - [14] S. K. Bogner, A. Schwenk, T. T. S. Kuo and G. E. Brown, nucl-th/0111042.
 - [15] S. K. Bogner, A. Schwenk, R. J. Furnstahl and A. Nogga, Nucl. Phys. **A763**, 59 (2005).
 - [16] A. Nogga, S. K. Bogner and A. Schwenk, Phys. Rev. C **70**, 061002(R) (2004).

- [17] F.A. Berezin, G.P. Pochli and V.M. Finkelberg, Moscow Univ. Vestnik **1**, 21 (1964); J.B. McGuire, J. Math. Phys. **5**, 622 (1964); E. Brezin and J. Zinn-Justin, C.R. Acad. Sci. (Paris) **B263**, 670 (1966); C.N. Yang, Phys. Rev. Lett. **19**, 1312 (1967) and Phys. Rev. **168**, 1920 (1968); F. Calogero and A. Degasperis, Phys. Rev. **A11**, 265 (1975).
- [18] W. Glöckle, *The Quantum Mechanical Few-Body Problem* (Springer-Verlag, Berlin, 1983).